

86 GHz SiO maser survey of late-type stars in the Inner Galaxy

★,★★,★★★,†

I. Observational data

M. Messineo¹, H. J. Habing¹, L. O. Sjouwerman², A. Omont³, and K. M. Menten⁴

¹ Leiden Observatory, P.O. Box 9513, 2300 RA Leiden, the Netherlands
e-mail: messineo@strw.leidenuniv.nl; habing@strw.leidenuniv.nl

² National Radio Astronomy Observatory, P.O. Box 0, Socorro NM 87801, USA
e-mail: lsjouwerman@aoc.nrao.edu

³ Institut d'Astrophysique de Paris, CNRS, 98bis Boulevard Arago, F 75014 Paris, France
e-mail: omont@iap.fr

⁴ Max-Planck-Institut für Radioastronomie, Auf dem Hügel 69, D-53121 Bonn, Germany
e-mail: kmenten@mpifr-bonn.mpg.de

Received June xx, 2002; accepted xxxxxx xx, xxxx **Version October 31, 2018**

Abstract. We present 86 GHz ($v = 1, J = 2 \rightarrow 1$) SiO maser line observations with the IRAM 30-m telescope of a sample of 441 late-type stars in the Inner Galaxy ($-4^\circ < l < +30^\circ$). These stars were selected on basis of their infrared magnitudes and colours from the ISOGAL and MSX catalogues. SiO maser emission was detected in 271 sources, and their line-of-sight velocities indicate that the stars are located in the Inner Galaxy. These new detections double the number of line-of-sight velocities available from previous SiO and OH maser observations in the area covered by our survey and are, together with other samples of e.g. OH/IR stars, useful for kinematic studies of the central parts of the Galaxy.

Key words. stars: AGB and post-AGB – stars: late-type – circumstellar matter – surveys – masers – Galaxy: kinematics and dynamics

1. Introduction

There has been a growing interest in studies characterizing the kinematics and the spatial distribution of stars in the Inner Galaxy ($30^\circ < l < -30^\circ$). Many recent studies attempt to determine the parameters that describe the

dynamics and structure of the Inner Galaxy, i.e. its central bar and/or its bulge tri-axial mass distribution.

One approach is to map the spatial density of a stellar population. This has been done, e.g., for stars detected by IRAS toward the Galactic bulge (Nakada et al. 1991; Weinberg 1992), bulge Mira variables (Whitelock 1992), bulge red clump stars (Stanek et al. 1994) and giant stars seen in fields at symmetric longitudes with respect to the Galactic centre (Unavane & Gilmore 1998).

Optical studies of the Inner Galaxy are much hindered by the high interstellar extinction, which can exceed $A_V \approx 30$ (e.g. Schultheis et al. 1999), and thus are limited to small optical windows (Holtzman et al. 1998; Zhao et al. 1994). At infrared and radio wavelengths however, interstellar extinction is much less severe, or even absent. Extensive infrared point source catalogues have recently become available from the ground based DENIS (Epchtein et al. 1994) and 2MASS (Beichman et al. 1998) near-infrared (nIR) surveys, the mid-infrared (mIR) ISO satellite survey (ISOGAL: Omont et al. 1999; Omont & the ISOGAL collaboration 2002), and the Midcourse

Send offprint requests to: M. Messineo

* Based on observations with ISO, an ESA project with instruments funded by ESA member states and with the participations of ISAS and NASA.

** Based on observations carried out with the IRAM 30-m telescope located at Pico Veleta. IRAM is supported by INSU/CNRS (France), MPG (Germany) and IGN (Spain).

*** This is paper no. 16 in a refereed journal based on data from the ISOGAL project.

† The full Tables 2 and 3 are only available in electronic form at the CDS via anonymous ftp to [cdsarc.u-strasbg.fr](ftp://cdsarc.u-strasbg.fr) (130.79.128.5) or via [http://cdsweb.u-strasbg.fr/cgi-bin/qcat?J/A+A/\(vol\)/\(page\)](http://cdsweb.u-strasbg.fr/cgi-bin/qcat?J/A+A/(vol)/(page)). The complete Figure 7 is available only in electronic form at EDP Sciences via <http://www.edpsciences.org>.

Space Experiment (MSX; Egan et al. 1999; Price et al. 1997). These data have given new insights into the *spatial* stellar density distribution in the Inner Galaxy. To interpret the information given by the recent observations, detailed models all include some kind of tri-axiality: a tri-axial Galactic bulge or bar (e.g. Alard 2001; Debattista et al. 2002; López-Corredoira et al. 2001a,b; Ortwin 2002). However, the bar characteristics such as length, pattern speed, and position angle, are still poorly constrained.

Spatial density studies often neglect an important measurable dimension of phase space: the stellar line-of-sight velocity. In contrast to the large number of data points in the spatial domain of phase-space, the available data on the line-of-sight velocities of the stars is sparse because it is still difficult to measure velocities from optical or infrared studies. Asymptotic Giant Branch (AGB) stars with large mass-loss are a valuable exception, since their envelopes often harbour masers which are strong enough to be detected throughout the Galaxy and thereby reveal the line-of-sight velocity of the star to within a few km s^{-1} ; frequently detected maser lines are from OH at 1.6 GHz, H_2O at 22 GHz, and SiO at 43 GHz and 86 GHz (for a review see Habing 1996). Previous SiO and OH maser surveys in the Galaxy have demonstrated that locating the circumstellar masers is an effective way to measure line-of-sight velocities of the AGB stars (e.g. Baud et al. 1979; Blommaert et al. 1994; Deguchi et al. 2000a,b; Izumiura et al. 1999; Lindqvist et al. 1992; Sevenster et al. 1997a,b, 2001; Sjouwerman et al. 1998).

Until recently, only a few hundred stellar line-of-sight velocities were known toward the inner regions of the Milky Way ($30^\circ < l < -30^\circ$ and $|b| < 1$), mainly from OH/IR stars, AGB stars with OH maser emission in the 1612 MHz line, mostly undetected at visual wavelengths. This number is too small to allow for a good quantitative multicomponent analysis of the Galactic structure and dynamics (Vauterin & Dejonghe 1998). Obtaining more line-of-sight velocities therefore remains an issue of prime importance. However, masers are rare among stars, because sustaining a maser requires a special physical environment. Most of the mid-infrared brightest OH/IR stars close to the Galactic plane were probably already detected in the blind OH surveys or in the targeted OH or 43 GHz SiO maser observations of colour-selected sources from the IRAS survey (e.g. van der Veen & Habing 1988). H_2O surveys (e.g. Levine 1995) are probably incomplete because the H_2O masers are strongly variable.

SiO maser emission is detected from several transitions towards oxygen-rich AGB stars and red supergiants. On the basis of the shape and the amplitude of their visual light curve AGB stars have been classified as semi-regular (SR) stars and Mira stars. Variable AGB stars may also be classified as long period variable (LPV) stars, when their periods are longer than 100 days (Habing 1996). Almost all OH/IR stars are variable and have periods longer than 500 days. In the IRAS color-color diagram the oxygen-rich AGB stars are distributed on a well-defined sequence of increasing shell opacity and stellar mass-loss rate (e.g.

Olson et al. 1984; van der Veen & Habing 1988), which goes from Miras with the bluest colors and the $9.7 \mu\text{m}$ silicate feature in emission, to OH/IR stars with the reddest colors and the $9.7 \mu\text{m}$ silicate feature in absorption. The relative strengths of different SiO maser lines are observed to vary with AGB type (Bujarrabal et al. 1996; Nyman et al. 1993, 1986), indicating that the SiO maser properties depend on the stellar mass loss rate and on the stellar variability. The ratio of the SiO maser intensities of 43 over 86 GHz is found to be much lower in Mira stars and in supergiants than in OH/IR stars. This implies that the 86 GHz ($v = 1$) SiO maser transition is a good tool to measure stellar line-of-sight velocities of Mira-like stars. Another advantage is that Mira stars are far more numerous than OH/IR stars. However, these conclusions are based on small number statistics, and have neglected effects of variability.

To significantly enlarge the number of known stellar line-of-sight velocities we have conducted a targeted survey for the 86 GHz SiO ($v = 1, J = 2 \rightarrow 1$) maser line toward an infrared selected sample of late-type stars. Here we describe the selection of sources and the observational results. A detailed discussion of the kinematic and physical properties of the detected stars will be addressed in a forthcoming paper (Messineo et al. 2002a, in preparation). All velocities in this paper refer to line-of-sight velocities, measured with respect to the Local Standard of Rest (LSR).

2. Source selection

The stars to be searched for maser emission were selected from a preliminary version of the combined ISOGAL-DENIS catalogue and from the MSX catalogue. The search was limited to the Galactic plane between $l = -4^\circ$ and $l = +30^\circ$ and $|b| \lesssim 1^\circ$; the lower limit in longitude is imposed by the northern latitude of the IRAM 30-m telescope.

ISOGAL is a 7 and $15 \mu\text{m}$ survey made with ISOCAM on board of ISO of $\sim 16 \text{ deg}^2$, in selected fields along the Galactic plane, mostly toward the Galactic centre. The 7 and $15 \mu\text{m}$ observations were generally taken at different epochs. With a sensitivity of 10 mJy (two orders of magnitude deeper than IRAS) and a resolution of $3\text{--}6''$ ISOGAL detected over 100,000 objects. The combination of the mIR data with the I , J , and K_S -band DENIS photometric catalogue (Epchtein et al. 1994) allows for a good determination of the nature of these sources. ISOGAL has sampled the AGB population in the Galactic bulge ranging from the highly obscured, mIR luminous OH/IR stars, to the lower mass-loss Mira and SR stars near the tip of Red Giant Branch, at $K_o \sim 8.2$ at the adopted distance of 8.0 kpc to the Galactic centre (Alard et al. 2001; Glass 2000; Omont et al. 1999; Ortiz et al. 2002). The Midcourse Space Experiment (MSX) is a survey at five mIR wavelengths (from $4.3 \mu\text{m}$ [B1 band], to $21.4 \mu\text{m}$ [E band]) which covers the entire Galactic plane to $\pm 5^\circ$ Galactic latitude (Egan et al. 1999). With a sensitivity of 0.1 Jy in

band A (8.28 μm) and a spatial resolution of 18.3'', the MSX Galactic plane survey detected more than 300,000 objects.

Since the ISOGAL survey only covered a limited number of small fields, the MSX survey was used to obtain a more even distribution of candidate maser sources in the area of interest. Figure 1 shows the location of the observed sources.

In the selection of targets, three important earlier observations were taken into account as a guideline:

- *SiO maser emission occurs more frequently towards M-type Mira stars than towards other AGB stars* (Bujarrabal 1994; Habing 1996; Haikala et al. 1994; Lewis 1990; Matsuura et al. 2000).
- *86 GHz SiO maser emission is fainter towards OH/IR stars than towards Mira stars* (Lewis 1990; Nyman et al. 1993, 1986). Nyman et al. (1993, 1986) found that the ratio of the 43 over 86 GHz ($v = 1$) SiO maser line flux is much higher for OH/IR stars, varying from 2 to 10 with increasing mass-loss rate, than for Mira stars (0.4) as found by Lane (1982). For typical 43 GHz maser line intensities measured for Galactic bulge OH/IR stars (Lindqvist et al. 1991; Sjouwerman et al. 2002a), and for the low 86 to 43 GHz line flux ratios generally seen towards OH/IR stars, such stars should be weak at 86 GHz and at the distance of the Galactic centre, while Mira stars should be stronger.
- *The SiO maser line flux correlates with the mIR continuum flux density* (Alcolea et al. 1989; Bujarrabal 1994; Bujarrabal et al. 1987; Jiang 2002). Previous studies have shown that the 43 GHz ($v = 1$ and $v = 2$) line peak intensity correlates with the (~ 7 –12 μm) mIR continuum flux density (Bujarrabal 1994). The mIR and maser intensities vary together during the stellar cycle. Measuring the respective flux densities at the maximum, Bujarrabal et al. (1987) found that the $\text{IR}_{8\ \mu\text{m}}/\text{SiO}_{43\ \text{GHz}, v=1}$ ratio is ~ 5 in O-rich Mira stars. The $\text{IR}_{12\ \mu\text{m}}/\text{SiO}_{86\ \text{GHz}, v=1}$ ratio was found to be ~ 10 , albeit with a large scatter, by Bujarrabal et al. (1996) in a sample of O-rich late-type stars.

These observations provided us with criteria for our target selection, such as a lower IR flux density limit in order to detect the maser and IR colours to exclude the high mass-loss AGB stars. To avoid OH/IR stars, for which kinematic data is already known, we compiled a list of known OH/IR stars by combining the catalogues of Sevenster et al. (1997a,b, 2001), Sjouwerman et al. (1998) and Lindqvist et al. (1992).

2.1. ISOGAL selection criteria

The ISOGAL catalogue lists the measurements at 7 and 15 μm in magnitudes, here indicated as [7] and [15], respectively. The magnitudes of the sources in the ISOGAL-DENIS catalogue were corrected for extinction using an extinction map derived from the DENIS data by Schultheis et al. (1999) and using the extinction ratios

$(A_V : A_I : A_J : A_K : A_7 : A_{15}) = (1 : 0.469 : 0.256 : 0.089 : 0.020 : 0.025)$ (Glass 2000; Hennebelle et al. 2001; Teysseier et al. 2002).

We cross-referenced the Galactic centre LPV positions (Glass et al. 2001, 0.5'' accuracy) with the ISOGAL-DENIS catalogues and found 180 possible counterparts out of 194 variables located in fields observed by ISOGAL. The missing sources can be explained by blending with other sources or by high background emission (the complete description of this cross-correlation will be the subject of a forthcoming paper). Analyzing the locations of the LPV stars in the different ISOGAL-DENIS colour-magnitude diagrams (e.g. Fig. 2 and Fig. 3), where extinction corrected values are indicated by the suffix "o", we found that in the $(K_o - [15]_o)$ versus $[15]_o$ colour-magnitude diagram the LPVs without OH masers separate well from the OH/IR stars (at $(K_o - [15]_o) \approx 4$; Fig. 2).

The OH/IR stars, having 10^2 to 10^3 times higher mass-loss rates than Mira stars, are the brightest objects at 15 μm and have $(K_o - [15]_o)$ colour redder than 4 mag (Ortiz et al. 2002). This colour is an excellent indicator of infrared emission by the stellar envelope (Omont et al. 1999).

We selected sources from the ISOGAL catalogue by their $[15]_o$ magnitude, and their $(K_o - [15]_o)$ and $([7]_o - [15]_o)$ colours. See the search boxes in Fig. 2 and 3. We excluded the brightest 15 μm sources, $[15]_o < 1.0$, and those with $([7]_o - [15]_o) < 0.7$ and with $(K_o - [15]_o) < 1.95$, since they are likely to be foreground stars. We further excluded sources with $[15]_o > 3.4$ since they are –given the general correlation of SiO maser emission and IR luminosity– likely to show SiO maser emission fainter than our detection limit of 0.2 Jy. Sources with $([7]_o - [15]_o) > 2.3$ were excluded since they are likely to be compact HII regions or young stellar objects (Felli et al. 2000; Schuller & the ISOGAL collaboration 2002), and those with $(K_o - [15]_o) > 4.85$ because they are likely to be OH/IR stars with a high mass-loss rate (Fig. 2) or young stellar objects. To conservatively avoid duplicating the OH maser line-of-sight data points, sources near (50'') a known OH maser were excluded.

As the final photometry of ISO has changed slightly from the preliminary input catalogue, 16 of the selected sources no longer obey the selection criteria strictly. 253 objects were observed from the selected ISOGAL-DENIS sources.

2.2. MSX selection criteria

Since the MSX catalogue gives the source flux density, F , in Jy, here we use this unit. Magnitudes are obtained adopting as zero points: 58.55 Jy in A (8.26 μm) band, 26.51 Jy in C (12.12 μm) band, 18.29 Jy in D (14.65 μm) band and 8.75 Jy in E (21.41 μm) band.

NIR data from DENIS or 2MASS was not available for the MSX sources at the time of our observations. For the source selection we used flux densities in the A

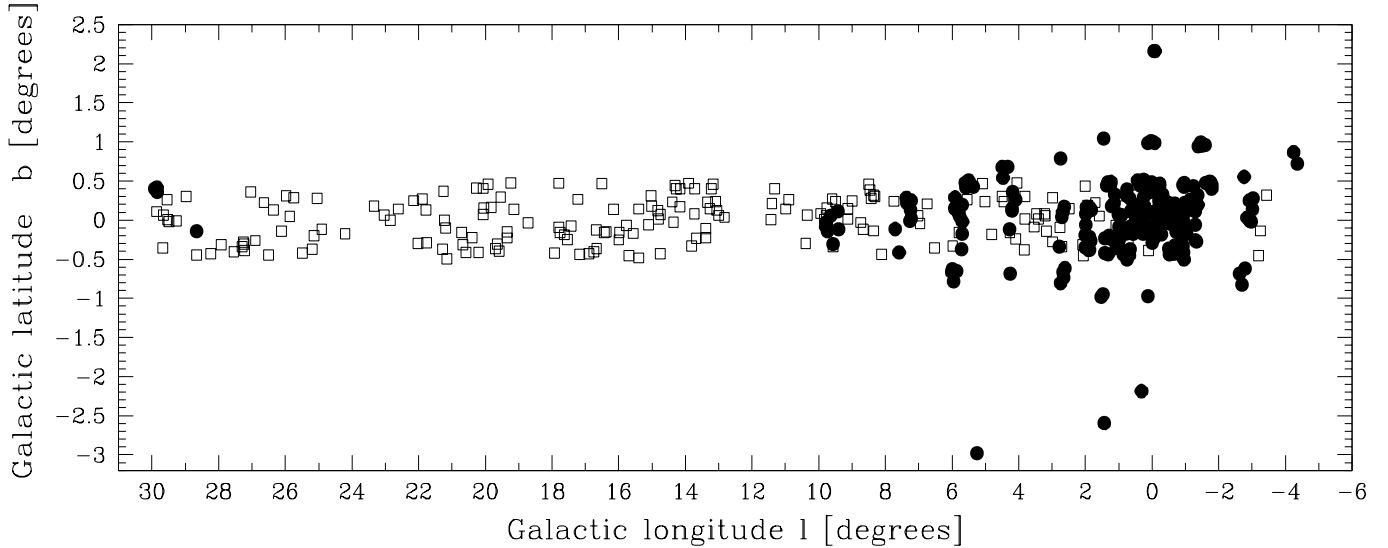


Fig. 1. Location of the observed sources, irrespective of detection and non-detections, in Galactic coordinates. The MSX sources are shown as open squares and the ISOGAL sources as filled circles.

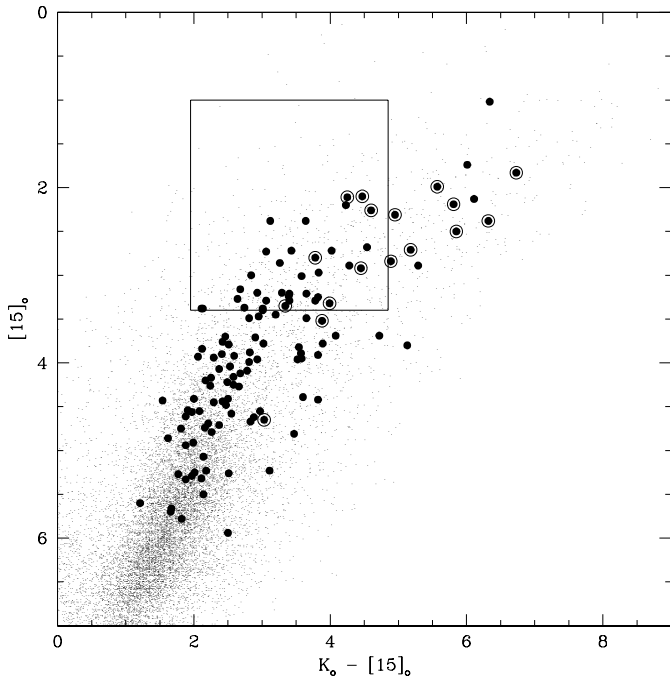


Fig. 2. $[15]_o$ versus $(K_o - [15]_o)$ ISOGAL-DENIS colour-magnitude diagram; extinction correction has been applied. LPV stars from Glass et al. (2001) are shown as big dots of which the encircled ones mark the variables with known OH maser emission. For comparison, the numerous small dots indicate all the ISOGAL sources within 5 degrees from the Galactic centre. The rectangular box defines the region of our sample. Note that the very red variables without OH emission to the right of the box in this figure correspond to outliers without OH emission in Fig. 3.

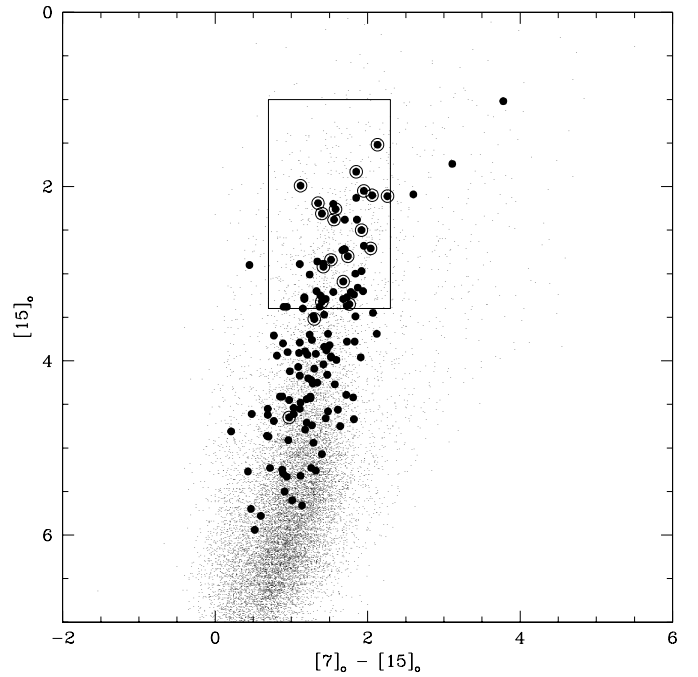


Fig. 3. $[15]_o$ versus $([7]_o - [15]_o)$ ISOGAL-DENIS colour-magnitude diagram; symbols as in Fig. 2. Note that a K_o is not known for all plotted sources, and they thus are missing in Fig. 2.

and D bands which have wavelength ranges similar to the ISOGAL 7 and 15 μm bands. We selected those not-

confused, good quality sources in band A and D ($\text{flag} > 3$), which show variability in band A. We avoided the reddest, $F_D/F_A > 2.29$, sources, which are likely to be OH/IR stars or young stellar objects, and the bluest and most luminous (likely foreground) stars with $F_D/F_A < 0.63$ and $F_D > 6$ Jy. Furthermore, following the work of Kwok et al. (1997) on IRAS sources with low-resolution spectra, we used the C to E band ratio to discard very red ($F_E/F_C > 1.4$) sources, which are likely to be young stel-

Table 1. IRAM 30-m observing dates

Period No.	Dates	JD-2450000
1	26-27 August 2000	1782-1783
2	04-17 December 2000	1882-1895
3	22-24 January 2001	1931-1933
4	09-24 February 2001	1949-1964
5	23-28 May 2001	2052-2057
6	15 August - 04 September 2001	2136-2156

lar objects or OH/IR stars with thick envelopes. Moreover, sources within 50 arcsec of a known OH maser were discarded, as the kinematic data are already known. We observed 188 sources from this MSX-selected sample.

3. Observations and data reduction

The observations were carried out with the IRAM 30-m telescope (Pico Veleta, Spain) between August 2000 and September 2001 (Table 1). Two receivers were used to observe the two orthogonal linear polarizations of the SiO ($v = 1, J = 2 \rightarrow 1$) transition at 86.24335 GHz. For each receiver we used one quarter of the low resolution, 1 MHz 1024 channel analog filter bank (3.5 km s^{-1} spectral resolution, and 890 km s^{-1} total velocity coverage), and in parallel the AOS autocorrelator at a resolution of 312.5 kHz (1.1 km s^{-1}) with a bandwidth of 280 MHz (973 km s^{-1} total velocity coverage). The telescope pointing errors were typically $2\text{--}4''$, which is small compared to the beam FWHM of $29''$. The observations were made in wobbler switching mode, with the wobbler throw varying between 100 and 200 arcsec. The on-source integration time was between 5 and 20 minutes per source, depending on the system temperature which varied between 100 and 300 K because of the weather, source elevation (typically 10 to 30°), and amount of continuum emission in the beam.

Flux calibration was done in a standard way from regular observations of a hot (ambient) and cold (liquid nitrogen) load. A sky-opacity-correction was computed from measuring the blank sky emissivity and using a model of the atmosphere structure. The conversion factor from antenna temperature to flux density changed from 6.0 to 6.2 Jy K^{-1} on December 12th 2000.

3.1. Flux stability

Two of the strongest SiO maser sources that were found in December 2000, were subsequently monitored in order to test them as possibly secondary flux calibrators. Figure 4 shows the measured source fluxes, in terms of antenna temperature, as a function of time over nine months. Within each observing period (up to a few weeks) the line flux measurements of the two sources are consistent within the measurement errors, with a typical day-to-day flux variation of 20 %. Over the whole period, however, the flux of the two sources varied up to a factor two. We did not notice variations of the average system temperature that might have caused systematic errors of this magni-

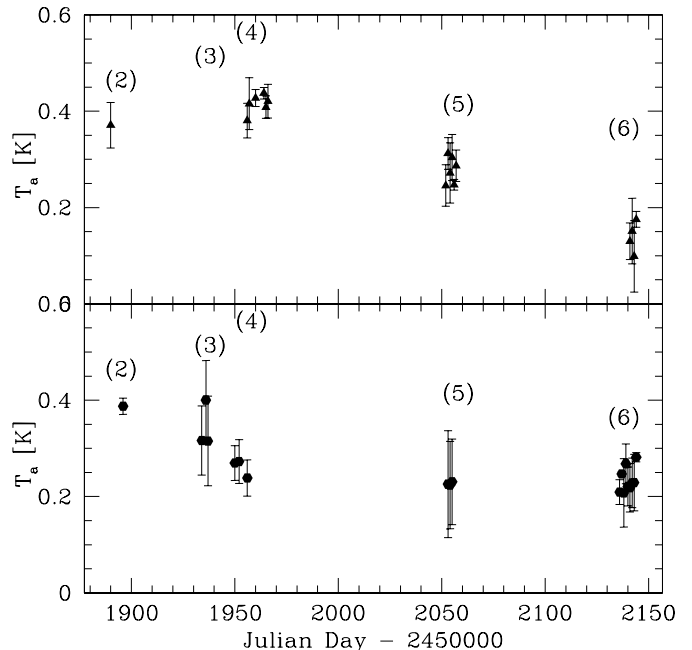


Fig. 4. Antenna temperatures versus time for the 2 ‘reference’ lines: sources #265 plotted with filled hexagons (bottom) and #163 with triangles (top). The observing date on the horizontal axis is expressed in Julian day minus 2450000. The labels refer to the observing periods in Table 1. The measurements of a single period agree within 20 %. A long term intrinsic variation (up to a factor of 2 in T_a) is apparent in both sources.

tude in the long-term flux calibration. The flux variation of both sources is therefore due to intrinsic source variability, and this makes these sources of limited use as long-term secondary flux calibrators. We shall adopt the observed short-term apparent flux variations as an indication of the absolute flux uncertainty for all our observations (i.e. $\lesssim 20$ %).

3.2. Detection criteria

The data were reduced using the CLASS software package. The spectra taken with the two receivers were combined, yielding a typical rms of 15 mK ($\sim 100 \text{ mJy}$) in the AOS channels. The line width (FWHM) and the integrated antenna temperature were determined by fitting the data from the autocorrelator with a gaussian after subtracting a linear baseline. Bad channels were eliminated by comparing the analog filter bank and autocorrelator spectra.

We considered as a detection only lines with peak antenna temperature greater than three times the rms noise level in the autocorrelator spectrum at the original resolution. Because of possible confusion with H^{13}CN lines, a problem discussed in the following subsection, single component emission lines detected at line-of-sight velocity less than -30 km s^{-1} were interpreted as SiO maser lines only if their line width is smaller than 7.5 km s^{-1} .

3.3. Confusion with interstellar $H^{13}CN$ emission

The total autocorrelator spectral bandwidth is 280 MHz, centered at the 86243.350 MHz rest frequency of the ($v = 1, J = 2 \rightarrow 1$) SiO maser transition. This observing band also includes the three ($J = 1 \rightarrow 0$) hyperfine transitions of $H^{13}CN$ at 86338.767, 86340.184, and 86342.274 MHz. The $H^{13}CN$ lines show up at velocity offsets of about -335 km s^{-1} ($-329, -336, -343 \text{ km s}^{-1}$) relative to the SiO line.

The $H^{13}CN$ line was observed in many interstellar clouds and also in the direction of Sgr A (e.g. Fukui et al. 1977; Hirota et al. 1998). In our spectra this $H^{13}CN$ line was also detected in the direction of the Galactic centre, at $3.5^\circ < l < -1.5^\circ, |b| < 0.5^\circ$, in 55 % of our pointings. $H^{13}CN$ spectra generally have multiple broad components and appear in absorption as well as in emission, depending on the line intensity in the on- and off-target position (Fig. 5). The (l, b) distribution of the spectra that contain the $H^{13}CN$ ($J = 1 \rightarrow 0$) line is similar to that of the Galactic centre molecular clouds, confirming that the origin is interstellar (see for example the ^{13}CO distribution in Fig. 2 of Bally et al. 1988). The $H^{13}CN$ line has been detected also from circumstellar envelopes of carbon stars (e.g. Dayal & Bieging 1995), but will not be detectable in AGB stars at the distance of the Galactic centre (e.g. Olofsson et al. 1998).

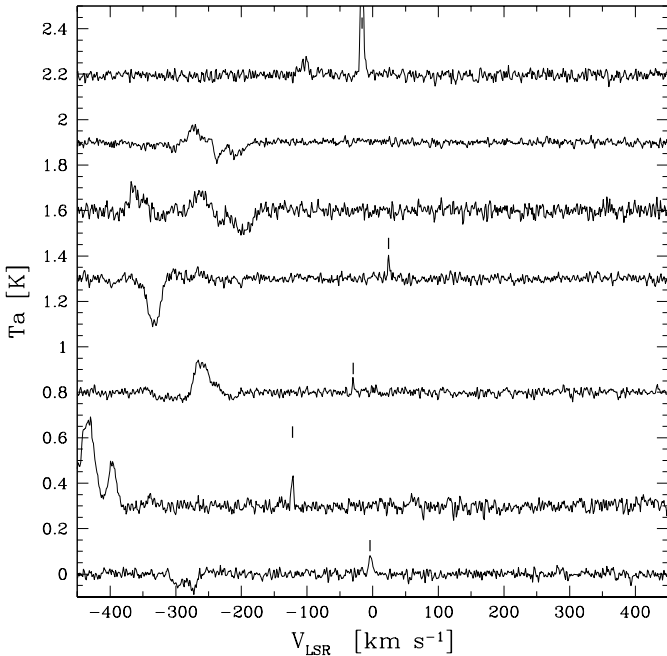


Fig. 5. Some spectra with interstellar $H^{13}CN$ emission, shown for clarity with arbitrary antenna temperature offsets. The small thick vertical bars indicate the detected SiO maser line. The $H^{13}CN$ and SiO lines are usually clearly distinct.

Considering that the maximum gas velocity observed in the Galactic centre is less than 300 km s^{-1} , for exam-

ple in the CO distribution (e.g. Dame et al. 2001), and considering the frequency differences between the three $H^{13}CN$ ($J = 1 \rightarrow 0$) hyperfine transitions and the SiO ($v = 1, J = 2 \rightarrow 1$) transition, the $H^{13}CN$ ($J = 1 \rightarrow 0$) line may be confused with SiO ($v = 1, J = 2 \rightarrow 1$) lines at velocities below -30 km s^{-1} . All lines detected at those velocities are therefore suspect and their line widths were examined in order to distinguish between SiO maser and $H^{13}CN$ lines. The typical line width of the $H^{13}CN$ and SiO emission is very different (Fig. 5). From the SiO lines detected at velocities larger than -30 km s^{-1} , i.e. where no confusion is expected, the SiO line width distribution ranges between 1.7 and 16.3 km s^{-1} with a peak at $\approx 4 \text{ km s}^{-1}$ (Fig. 6); the $H^{13}CN$ line is much wider and can be up to 100 km s^{-1} wide. With the spectral resolution of the AOS, 1 km s^{-1} , in case the $H^{13}CN$ emission is not spatially extended, one should be able to resolve two or three of the hyperfine components, which are separated by 7 km s^{-1} . We therefore identify a spectral line at velocity below -30 km s^{-1} as an SiO maser only if it is a single emission component and if its line width (FWHM) is narrower than 7.5 km s^{-1} . For an unambiguous SiO identification further observations would be required, e.g. by searching for the 43 GHz SiO maser lines, or by using interferometric 86 GHz observations to locate the position and to determine the extent of the emission.

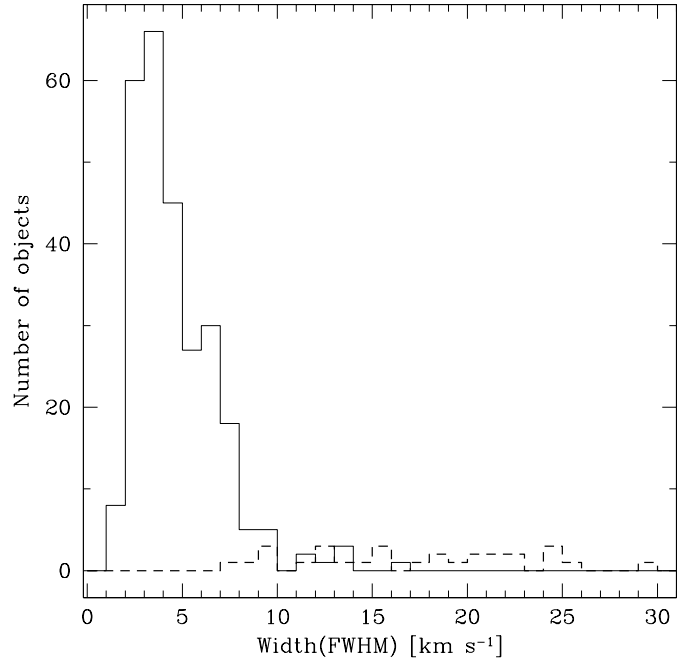


Fig. 6. Histogram of the line widths. The solid line shows the distribution of the SiO line widths; the dashed line shows the distribution of the lines with a single component in emission which we classified as $H^{13}CN$ emission.

We have probably rejected a few SiO lines because of suspected confusion with $H^{13}CN$. Of the 202 SiO lines detected at velocities larger than -30 km s^{-1} 25 (12 %) have widths larger than 7.5 km s^{-1} . Within 3° from the Galactic

centre, we found 75 SiO lines at velocities larger than -30 km s^{-1} ; while at velocities smaller than -30 km s^{-1} we found 51 emission line sources with widths $< 7.5 \text{ km s}^{-1}$ (SiO lines) and 29 emission lines with widths $> 7.5 \text{ km s}^{-1}$ and with single component which we conservatively classified as H^{13}CN . Considering the above 12 %, we estimate that we could have eliminated about 7 real SiO lines.

Only one spectrum taken at a position away from the central molecular complex shows a line which is classified as H^{13}CN emission (at $l = 23^\circ$ for source #423); this is further discussed in Sect. 4.6.

3.4. Confusion with interstellar SiO emission

In the interstellar medium almost all Si atoms are supposedly locked up in silicate dust particles. There is, however, some SiO emission seen towards interstellar molecular clouds (Lis et al. 2001; Martin-Pintado et al. 1992, 1997), in which case shocks have probably destroyed the refractory grain cores, releasing the silicon back into the gas phase.

However, our stellar SiO maser survey is little affected by confusion with this interstellar SiO emission for several reasons. First, we have targeted mIR sources. The bulk of the interstellar SiO emission in the Galactic centre is not associated with mIR radiation (Martin-Pintado et al. 1997). Furthermore, our SiO maser lines are generally narrower than the $10\text{-}50 \text{ km s}^{-1}$ found for shocked and energetic outflows associated with young stars. Young stellar objects would also be located in a different region of the colour-magnitude diagrams of Figs. 2 and 3 (Felli et al. 2000). Finally, follow-up observations with the Very Large Array (VLA) at 43 GHz have shown that 38 of 39 sources for which we detected 86 GHz SiO emission do also show unresolved 43 GHz SiO emission (Sjouwerman et al. 2002b, in preparation). It is therefore unlikely that any of this emission arises from interstellar molecular clouds.

We have also analyzed the 7 SiO lines (from Table 2) which have widths larger than 10 km s^{-1} (#113, #117, #129, #135, #173, #203, #223). They represent 2.5 % of our total number of detections and are located at longitudes between 2 and 18 degrees. The corresponding seven targeted mIR objects were all detected in the DENIS *K* band and some in the *J* band, and their IR colours are typical of late-type stars. Towards two of the sources, #113 and #117, we also detected H^{13}CN emission with a difference in radial velocity between the H^{13}CN and the 86 GHz SiO line of -42 and -22 km s^{-1} , respectively. The fit of the width of #113 is however noisy and can very well be less than 10 km s^{-1} or a blend of two lines. For #117 it could be a molecular cloud line, since a difference in radial velocity between the H^{13}CN and the SiO lines up to 25 km s^{-1} has been already observed towards molecular outflows (Martin-Pintado et al. 1992). However, #117 is clearly a $\lesssim 7 \text{ km s}^{-1}$ wide, 43 GHz ($v = 1$ and $v = 2, J = 1 \rightarrow 0$) SiO maser point source in our VLA follow-up observations (Sjouwerman et al. 2002b, in

preparation). We conclude that the mIR emission, and 43 and 86 GHz SiO lines are all related to an AGB star, although we cannot completely rule out interstellar H^{13}CN emission for source #117.

Two SiO emission features are probably of interstellar origin; see comments in Sec. 4.6 for remarks on the individual sources #94 and #288.

4. Results

Tables 2 and 3 summarize, in order of RA, our 271 SiO maser detections and 173 non-detections, respectively. The columns of Table 2 are as follows: an identification number (*ID*), followed by the Right Ascension (*RA*), and Declination (*DEC*), (in J2000) of the telescope pointing, the velocity of the peak intensity (V_{LSR}), as well as the peak antenna temperature (T_{a}) and the rms noise (*rms*), the integrated flux density (*A*) plus its formal error and the line width (*FWHM*) with its formal error, and finally the observing date (*Obs.Date*). If appropriate, comments are added in an extra column. The line width was calculated using a gaussian fit. Table 3, with the non-detections, lists only an identification number (*ID*), the *RA* and *DEC* of the telescope pointing, the achieved noise (*rms*) and the observing date (*Obs.Date*). An additional column is used for comments on individual pointings.

Figure 7 shows the spectra of the detected SiO ($J = 2 \rightarrow 1, v = 1$) lines. In each panel the spectrum obtained with the autocorrelator (lower spectrum) and the one obtained with the filter bank (upper spectrum) is given. The latter is shifted arbitrarily upwards for clarity.

The Table with all the additional IR measurements (from DENIS-ISOGAL and from MSX data) will follow in the next paper where the physical properties of the sources will be discussed (Messineo et al. 2002a, in preparation).

4.1. Detection rate

We have observed 441 positions, and detected SiO ($v = 1, J = 2 \rightarrow 1$) maser lines in 268 of them. Since 3 spectra show two SiO lines at different velocities (#21 and #22; #64 and #65; #77 and #78) the total number of detected lines is 271 (see Table 2 for the detections and 3 for non-detections). The total detection rate is 61%.

The spectra with two detections in one single beam are most probably detections of another AGB masing star by chance in the beam ($29''$) of our targeted sources (see Sec. 4.6). The number of these detections is a function of the stellar density: the three chance detections are located within 1° from the Galactic centre. Considering that chance detections are distributed randomly among the overall detections and non-detections of targeted sources, we deduce 6 as the number of chance detections within one degree from the Galactic centre. This corresponds to 5 % of the 123 observations performed in that region, which in total cover 86 square arcmin. The obtained spatial density of chance detections is consistent with the 43 GHz SiO maser density, 360 sources per square degree (8.5 sources

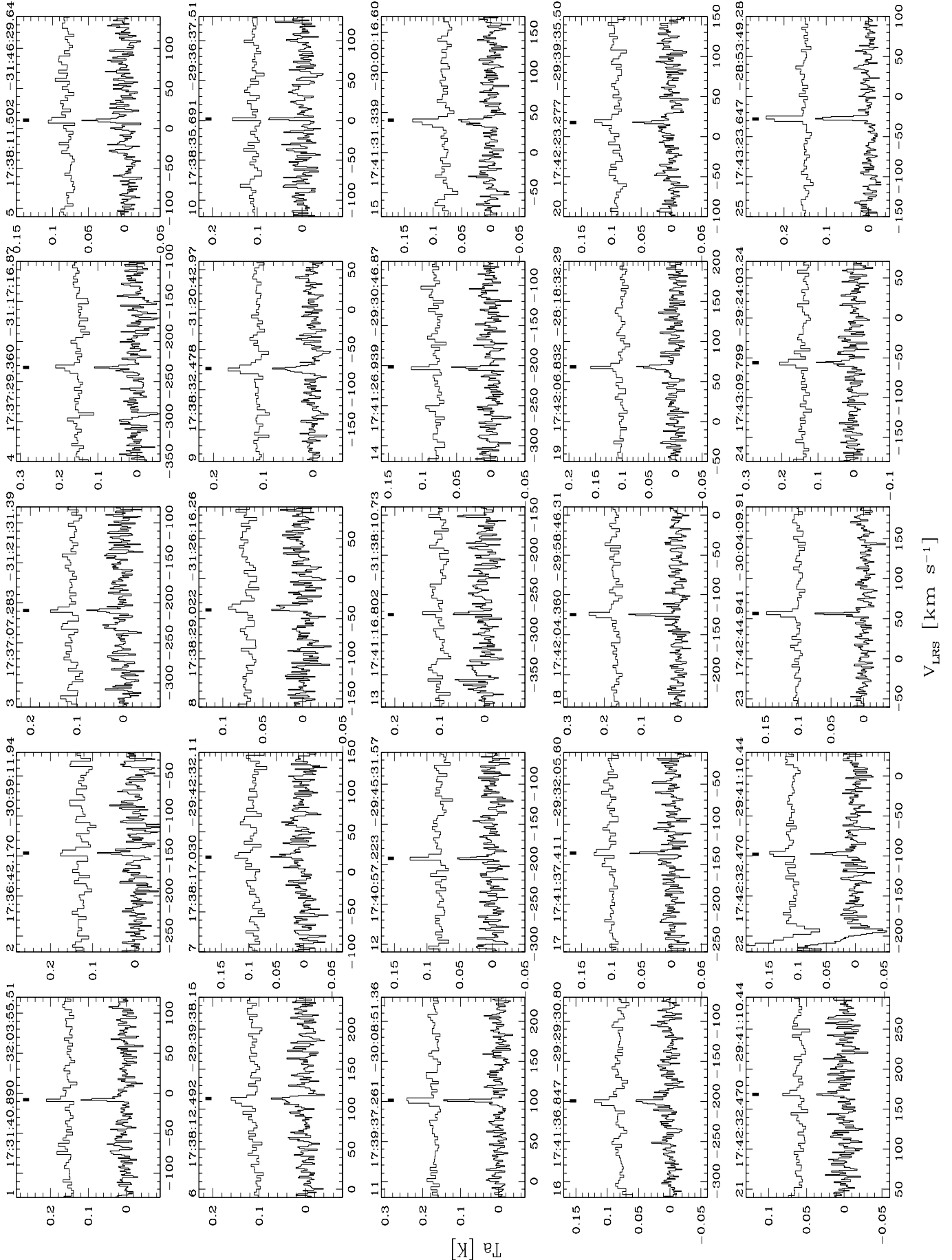


Fig. 7. Spectra of SiO ($J = 2 \rightarrow 1, v = 1$). Each panel shows the spectrum obtained with the autocorrelator (lower spectrum) and the one obtained with the filter bank (upper spectrum). The latter is shifted arbitrarily upwards for clarity. The full figure shows 271 spectra and is available only in the electronic version of the paper at <http://www.edpsciences.org>.

Table 2. Sources with SiO maser detected^{*,**}. The conversion factor from antenna temperature to flux density is 6.2 Jy K⁻¹.

ID	RA [J2000]	DEC [J2000]	V _{LRs} [km s ⁻¹]	T _a [K]	rms [K]	A [K km s ⁻¹]	FWHM [km s ⁻¹]	Obs.Date [yyymmdd]	Comments
1	17 31 40.9	-32 03 56	-8.3	0.120	0.018	0.34 ± 0.05	2.7 ± 0.5	010216	
2	17 36 42.2	-30 59 12	-146.2	0.089	0.023	0.26 ± 0.08	3.0 ± 1.4	010219	
3	17 37 07.3	-31 21 31	-209.2	0.079	0.017	0.26 ± 0.05	3.5 ± 0.9	010216	
4	17 37 29.4	-31 17 17	-232.0	0.110	0.023	0.52 ± 0.10	6.4 ± 1.5	010219	
5	17 38 11.5	-31 46 30	10.2	0.059	0.010	0.20 ± 0.03	3.5 ± 0.6	010524/010528	
6	17 38 12.5	-29 39 38	113.4	0.074	0.017	0.48 ± 0.07	7.9 ± 1.3	010526	
7	17 38 17.0	-29 42 32	18.9	0.060	0.015	0.36 ± 0.10	8.3 ± 4.1	010822	
8	17 38 29.0	-31 26 16	-38.7	0.039	0.011	0.22 ± 0.04	6.3 ± 1.1	010219/010903	
9	17 38 32.5	-31 20 43	-73.4	0.082	0.013	0.45 ± 0.05	6.4 ± 0.8	000827	29716 ^b
10	17 38 35.7	-29 36 38	1.5	0.074	0.018	0.21 ± 0.04	2.2 ± 0.4	010523	

* The full table contains 271 objects and is available in electronic form at the CDS via anonymous ftp to cdsarc.u-strasbg.fr (130.79.128.5) or via [http://cdsweb.u-strasbg.fr/cgi-bin/qcat?J/A+A/\(vol\)/\(page\)](http://cdsweb.u-strasbg.fr/cgi-bin/qcat?J/A+A/(vol)/(page)).

** Question marks denote marginal detections (T_a/rms < 3.5).

^a Identification number from Table 2 of Glass et al. (2001).

^b Identification number from Table 2 of Schultheis et al. (2000).

Table 3. Sources with no SiO maser detected*. The conversion factor from antenna temperature to flux density is 6.2 Jy K⁻¹.

ID	RA [J2000]	DEC [J2000]	rms [K]	Obs.Date [yyymmdd]	Comments
272	17 31 57.6	-32 14 11	0.018	010216	
273	17 35 56.2	-31 40 42	0.016	010528	
274	17 37 04.2	-27 52 04	0.017	010523	
275	17 37 07.7	-27 51 06	0.016	010523	
276	17 37 42.9	-31 24 56	0.021	010216	
277	17 38 01.6	-29 46 60	0.010	000827	
278	17 38 26.5	-31 28 22	0.011	010815	
279	17 39 29.8	-30 10 20	0.011	010219/010903	
280	17 39 30.4	-30 13 33	0.012	000826	41172 ^b
281	17 39 30.7	-30 08 50	0.016	010219	37877 ^b
282	17 39 35.7	-31 53 42	0.019	010523	

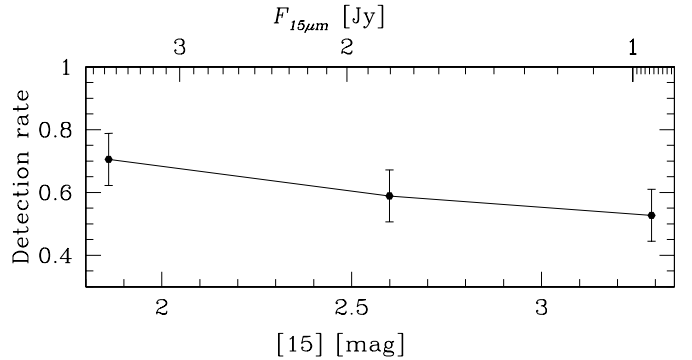
* The full table contains 173 objects and is available in electronic form at the CDS via anonymous ftp to <ftp://cdsarc.u-strasbg.fr> or via [http://cdsweb.u-strasbg.fr/cgi-bin/qcat?J/A+A/\(vol\)/\(page\)](http://cdsweb.u-strasbg.fr/cgi-bin/qcat?J/A+A/(vol)/(page)).

^a Identification number from Table 2 of Glass et al. (2001).

^b Identification number from Table 2 of Schultheis et al. (2000).

in 86 square arcmin), obtained in the Galactic centre by Miyazaki et al. (2001). This indicates that any blind survey will be less efficient than a targeted survey even in the central few degrees of our Galaxy.

The SiO maser detection rate tends to slightly increase with the mIR flux density at 7 and 15 μ m. In Fig. 8 we show the detection rate as function of the (ISOGAL) magnitude at 15 μ m, [15], or the MSX D band magnitude if no 15 μ m ISOGAL magnitude is available. The detection rate is 71 % for the bright mIR sources at magnitude [15] \sim 1.8 (\sim 3.8 Jy), and decreases to 53 % for the less bright mIR sources at magnitude [15] \sim 3.2 (\sim 1 Jy).

**Fig. 8.** Detection rate as a function of the magnitude at 15 μ m (ISOGAL [15] or MSX D band). Each bin contains \sim 145 sources.

We detected SiO maser emission in 143 out of 253 targets observed from the ISOGAL catalogue (57 %). The MSX targets give a higher detection rate: 125 detections out of 188 sources (66 %). This is due to the correlation between the mIR flux density and the detection rate and to the different sensitivity of the ISOGAL and MSX surveys. In fact, the ISOGAL sources were selected to have magnitude at 15 μ m lower than 3.4, i.e., flux density larger

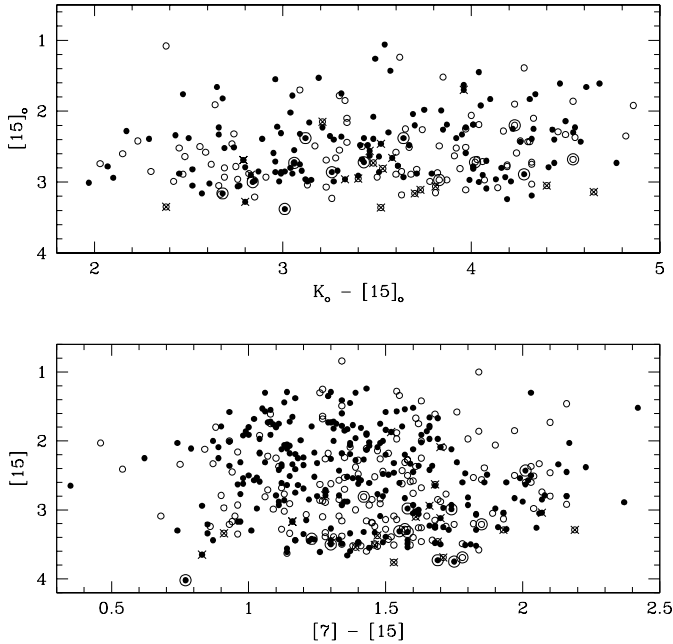


Fig. 9. Lower panel: $[15]$ versus $([7] - [15])$ colour-magnitude diagram; where ISOGAL magnitudes, or the A and D MSX magnitudes if no ISOGAL magnitude is available, are used. Upper panel: $[15]_o$ versus $(K_o - [15]_o)$ ISOGAL-DENIS extinction corrected colour-magnitude diagram. Detections are shown as filled circles; non-detections as open circles. The LPVs from Glass et al. (2001) are marked with a larger open circle, whereas the sources from Schultheis et al. (2000) are marked with crosses. Note that two points fall outside the figure.

than ~ 800 mJy, while most of the MSX targets have a flux density in the D band higher than 1.5 Jy. If we restrict our analysis to the brightest ISOGAL sources ($F_{15} > 1.5$ Jy, $[15] < 2.75$), we find similar results for both samples.

4.2. Variability

We observed 15 LPVs found by Glass et al. (2001) and detected SiO maser emission from 11 of them (73 %). Since the observations were taken at a random pulsation phase and since the SiO maser intensity is known to vary during the stellar phase by up to a factor ten (Bujarrabal 1994), this detection rate is a lower limit to the actual percentage of LPV sources characterized by 86 GHz SiO maser emission. Only 16 % of those LPV stars have associated OH emission (Glass et al. 2001), and among those within our defined colour-magnitude regions only 23 %. Among large amplitude variable AGB stars the 86 GHz SiO masers are much more frequent than OH masers.

Our sample of ISOGAL-DENIS sources also includes 19 sources from a list of Schultheis et al. (2000) of candidate variable stars, which were selected on the basis of repeated observations within the DENIS survey. We detected SiO maser emission in 8 of those stars. The low detection rate in these candidate variable stars may be

due to their low mIR brightness, $[15] \sim 3.2$ (see Fig. 9 and 8), and the uncertain indication of variability.

For the rest of our sources the only available information on variability is given by the photometric flag in the MSX catalogue (Egan et al. 1999). The sources we selected from the MSX catalogue all have an indication of variability in band A. Of the ISOGAL-selected sources with a MSX counterpart (Messineo et al. 2002a, in preparation), about half show variability in at least one MSX band. The ISOGAL catalogue does not contain any variability information. Alard et al. (2001) have combined ISOGAL and MACHO data in Baade’s Windows and found that 90 % of the objects detected in the MACHO and ISOGAL show well-defined variability (SR and Mira stars); however, for most SRs the amplitude of the variation is small. The Mira stars among these are generally the most luminous dust emitters (Fig. 1 in Alard et al. 2001). With $[15] < 3.4$, our sources are brighter than the Mira stars in Baade’s Windows, the latter having shorter periods than the Galactic centre LPVs and lower luminosity (Blum et al. 1996; Glass et al. 2001). Thus, most of our sources are probably strongly variable long period AGB stars. Follow-up variability studies are recommended.

4.3. Line intensity

In spite of the many observational studies of SiO maser emission, its pumping mechanism is still unclear. Previous 43 GHz SiO maser and mIR observations show a linear correlation between the respective flux densities (Bujarrabal et al. 1996, 1987; Jiang 2002; Nyman et al. 1993). This correlation argues in favor of radiative pump of the SiO masers, and against collisional pumping models. The average ratio between the 86 GHz SiO ($v = 1$) maser peak intensity and the $12 \mu\text{m}$ IRAS flux density is 0.1, though with a large scatter (Bujarrabal et al. 1996).

The dotted line in Fig. 10 is the best fit found by Jiang (2002) between the 43 GHz SiO maser intensity and the MSX band A flux density. Our results do not constrain the linear relation between the SiO maser and the mIR flux densities. Unfortunately, our data are not suitable to study this relation because the SiO intensity distribution is limited by sensitivity and the data span less than one order of magnitude of the mIR flux density, which is narrower than the data of previous work. The scatter is caused partly by the intrinsic source variability and the non-simultaneity of the mIR and SiO maser observations, and partly by a wide range of source distances. We looked at the distance effects considering the magnitudes $\log(F_{\text{SiO}}/F_D)$ and $\log(F_A/F_D)$, which are independent of the distance, and we obtained a similar scattered diagram.

4.4. Longitude-velocity diagram

In Figure 11 we compare the longitude-velocity ($l - v$) distribution of our SiO maser stars with that of the ^{12}CO line emission (Dame et al. 2001). The gas kinematics is a

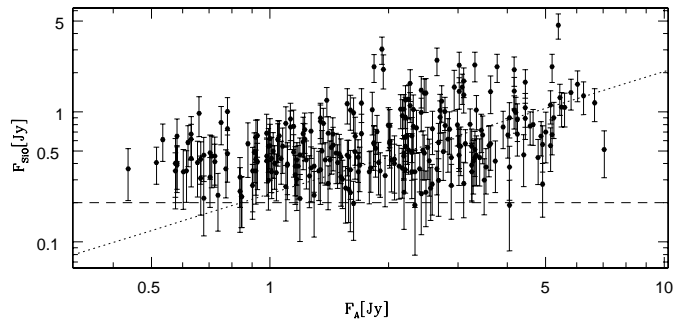


Fig. 10. 86 GHz SiO peak intensity as a function of MSX A band or ISOGAL 7 μm flux density. The dashed horizontal line shows the average 3σ detection limit. The dotted line shows the relation obtained by Jiang (2002) from 43 GHz data.

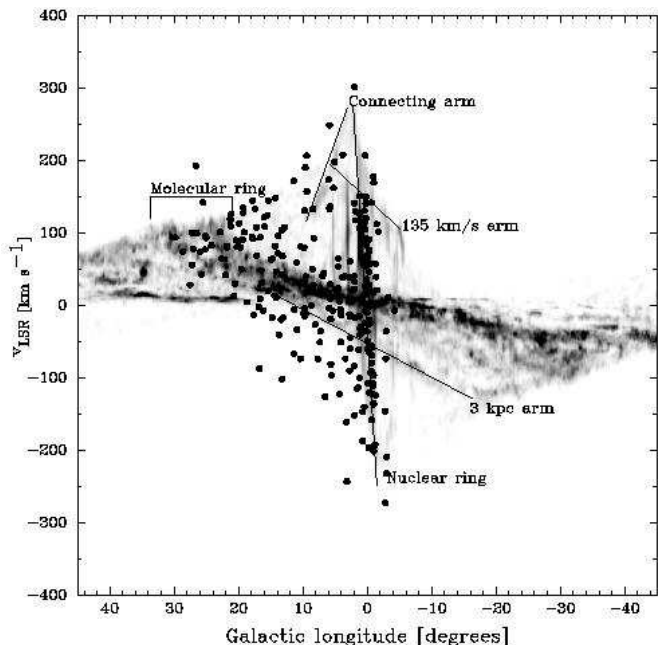


Fig. 11. Stellar longitude-velocity diagram overlaid on the grayscale CO ($l-v$) diagram from Dame et al. (2001). The SiO 86 GHz masers are shown as dots.

good tracer of the dynamical mass in the Galaxy. Main features of the distribution of the CO in the Inner Galaxy are labelled in Fig. 11, following Fig. 1 of Fux (1999). The line-of-sight velocities of our SiO maser sources range from -274 to 300 km s^{-1} , consistent with previous stellar maser measurements and with the CO velocities. An appreciable number of SiO sources are away from the CO emission contours, in a region forbidden for pure circular rotation, at negative velocities between $20^\circ > l > 0^\circ$. Around longitude 0° the stellar distribution follows the high velocity gas component of the nuclear disk. Similar results were found by Sevenster et al. (2001). We defer a more detailed analysis of the kinematic properties of the new SiO maser sample to a future paper.

In Figure 12 we have marked, as open circles, the location of the H^{13}CN lines we detected at velocities smaller

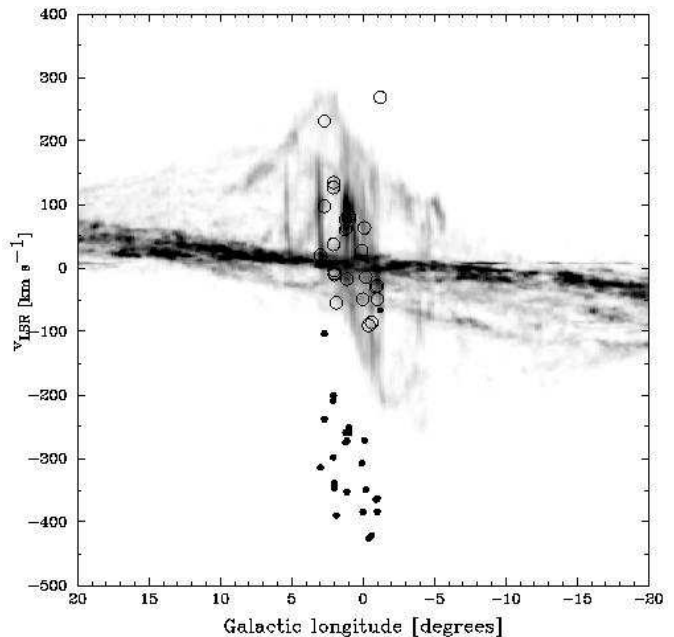


Fig. 12. The grayscale is the CO ($l-v$) diagram from Dame et al. (2001). The open circles indicate H^{13}CN lines, their location is in agreement with the CO distribution. The dots represent the position of the same lines if considered as SiO lines. The ($l-v$) diagram confirms the interstellar origin of those lines. The open circle located above the CO distribution at $l = -1.2$ (source #288) is discussed in Sec. 4.6.

than -30 km s^{-1} with widths wider than 7.5 km s^{-1} . Their distribution mostly follows the central gas distribution, confirming their interstellar origin and the validity of the adopted classification criteria based on the line width.

4.5. Comparison with previous detections

All OH/IR stars from the catalogues by Sevenster et al. (1997a,b, 2001); Sjouwerman et al. (1998) and Lindqvist et al. (1992) were excluded from our target list since their velocities are already known from the OH maser lines. Besides, previous studies (Nyman et al. 1993, 1986) anticipate a low detectability of 86 GHz SiO masers in OH/IR stars toward the Galactic centre, which also seems to be consistent with the results of our recent 30-m IRAM survey for 86 GHz SiO masers in Galactic center OH/IR stars Messineo et al. (2002b), in preparation.

4.5.1. Nobeyama 43 GHz surveys

There is a small overlap between the regions observed for the Japanese 43 GHz SiO maser surveys of IRAS point sources (Deguchi et al. 2000a,b; Izumiura et al. 1999) and the region observed for our survey. Using a search radius of $25''$ around each of our sources, which is about half the 43 GHz main beam at the Nobeyama telescope and almost the full 86 GHz beam of the IRAM 30-m, we found 19 matches between our positions and the IRAS sources

positions (Table 4). The velocities at 86 and 43 GHz of 7 sources detected in both lines agree within a few km s^{-1} . Source #256 (IRAS 18301-0900) shows a difference of 8 km s^{-1} between the SiO maser line at 43 GHz and at 86 GHz, but this source clearly has a double peak in the 43 GHz spectrum and the 86 GHz peak corresponds to one of the 43 GHz peaks. The low number of sources which are detected in both surveys needs further study, but can partially be due to source variability. Considering those 19 sources in common between the two surveys, the SiO maser detection rate appears higher at 43 GHz (68 %) than at 86 GHz (52 %). However, this small sample of sources is not representative of our full sample and of our 86 GHz SiO maser detection rate (66 % for MSX); it is biased toward redder A-D colour (higher mass-loss rate).

Table 4. Overlap between our 86 GHz SiO maser survey and the 43 GHz SiO maser survey in IRAS sources by Deguchi et al. (2000a,b); Izumiura et al. (1999). Column (1) lists the source ID number, column (2) the IRAS name, column (3) the 86 GHz line-of-sight velocity, column (4) the 43 GHz line-of-sight velocity and column (5) the separation between the IRAS position and our position.

ID	IRAS	V_{LSR} [km s^{-1}]		separation [arcsec]
		86 GHz	43 GHz	
72	17429–2935	2.6	−0.8	22.2
125	17497–2607	−162.5	−163.1	7.6
141	17524–2419	196.0	no det	10.8
154	17563–2402	136.2	no det	15.9
162	17586–2329	−125.6	no det	7.6
166	18000–2127	134.1	134.1	6.1
187	18056–1923	−34.3	−32.2	8.7
197	18106–1734	−16.9	−16.7	21.6
236	18229–1122	112.3	111.4	4.5
256	18301–0900	101.5	109.6	5.5
361	17483–2613	no det	163.2	7.0
363	17492–2636	no det	88.8	14.9
365	17497–2608	no det	no det	4.7
371	17509–2516	no det	−93.8	5.3
400	18037–2026	no det	68.2	6.4
411	18167–1517	no det	no det	12.3
417	18238–1135	no det	180.0	6.9
418	18246–1125	no det	80.0	2.8
423	18302–0848	no det	no det	9.2

To avoid saturation of the detector, the very centre of the Galaxy was not observed by ISOGAL (see Ortiz et al. 2002). Therefore, none of our sources is located in the regions centered on SgrA, which were mapped at 43 GHz by Miyazaki et al. (2001) and Deguchi et al. (2002).

Imai et al. (2002) report 43 GHz SiO maser detections towards LPV stars found by Glass et al. (2001). Seven LPV stars detected at 43 GHz coincide with sources

in our 86 GHz SiO maser survey (#48 = g23–5, #49 = g23–8, #52 = g21–39, #56 = g22–11, #73=g6–25, #80=g14–2, #332=g12–21). In 4 cases there is a corresponding SiO maser detection in the 86 GHz spectrum at a velocity consistent with the 43 GHz line. Sources #80 and #49 were both detected at 86 GHz, but there is a significant difference between the 86 and 43 GHz velocities of 7 and 17 km s^{-1} , respectively. The reason for this is unclear because the 43 GHz spectra were not published in Imai et al (2002). Finally, #332 was detected at 43 but not at 86 GHz, which is probably due to source variability.

4.5.2. 43 GHz SiO masers in the Sagittarius B2 Region

Table 5. Cross identification with sources detected by Shiki et al. (1997). Reference numbers from Shiki et al. (1997) and our names are listed in column 1, and 2 respectively. The separation from the closest ISOGAL source and its name in column 3 and 4. Finally the velocities at 43 and 86 GHz in columns 8 and 9. Shiki’s source number 2 is not in the ISOGAL catalogue prepared for the first release, but it is clearly a strong source in the ISOGAL image, and probably is associated with a foreground supergiant (Shiki et al 1997).

REF	ID	separation [arcsec]	ISOGAL name	V_{LRS} [km s^{-1}]	
				43 GHz	86 GHz
1	88	6.51	<i>PJ174656.2–283105</i>	56.5	55.8
2				−25.7	
3		2.03	<i>PJ174720.3–282305</i>	82.3	
4		7.19	<i>PJ174812.0–281817</i>	80.9	
5		16.46	<i>PJ174823.7–282018</i>	81.0	
6		10.56	<i>PJ174814.6–280852</i>	101.2	
7	99	6.95	<i>PJ174813.2–281941</i>	−38.7	−36.5

Shiki et al. (1997) mapped a subregion of Sgr B2 at 43 GHz and found seven SiO maser lines, only two of which could be identified with an IRAS source (Shiki’s #3 and #6). We found an ISOGAL counterpart within $17''$ in all cases, and from their mIR colours, we confirm that those seven detections are stellar maser sources in the line-of-sight of the giant molecular cloud Sgr B2. Two of those ISOGAL sources were observed in our 86 GHz survey, and for both sources the 43 and 86 GHz line velocities are consistent (see Table 5).

4.6. Comments on individual objects

#21 and #22

Sources #21 and #22 were detected in the same beam. The peak intensity of #21 is only 3 times the noise rms and we list the line as a marginal detection. However, a sec-

ond ISOGAL source, ISOGAL–PJ174232.9–294124, happened to fall inside the beam, at $15.6''$ from the position we targeted. This source is less bright at $15\ \mu\text{m}$ ($[15] = 4.73$) than the targeted ISOGAL–PJ174232.5–294110 ($[15] = 3.17$) and this suggests that the original targeted ISOGAL–PJ174232.5–294110 is the mIR counterpart of the stronger SiO line, #22, while ISOGAL–PJ174232.9–294124 is probably the counterpart of #21. Observations at 86 GHz and/or both of the 43 GHz SiO lines, at both stellar positions, may confirm our conclusion.

#64 and #65

Two very narrow SiO line sources #64 and #65 were detected in the same spectrum. Both lines have the same peak intensity, but different velocities, 53.7 and $-7.2\ \text{km s}^{-1}$, respectively. This suggests that the two lines are generated in the envelopes of two different AGB stars. The ISOGAL catalogue does not give another source within $30''$ of the position of targeted ISOGAL–PJ174528.8–284734, neither does inspection of the ISOGAL images at 7 and $15\ \mu\text{m}$. However, at that position there is strong background emission which may have limited detection of fainter stellar mIR sources.

#77 and #78

Sources #77 and #78 were detected in the same spectrum at velocities of 141.6 and $27.6\ \text{km s}^{-1}$, respectively. The targeted ISOGAL source, ISOGAL–PJ174618.9–284439, is separated by $12.5''$ from ISOGAL–PJ174619.5–284448. However, the latter is a weak mIR source only detected at $7\ \mu\text{m}$ ($[7] = 8.73$) by ISOGAL. Again, observing at 86 or 43 GHz at both stellar positions may resolve the mIR counterpart associated with the SiO maser line.

#94

This double peaked source is located in the Sgr B2 region. The two lines have similar intensities and are at velocities -36.6 and $-28.8\ \text{km s}^{-1}$ with respect to SiO (or 299.4 and 307.2 with respect to H^{13}CN), with widths of 5 and $3\ \text{km s}^{-1}$, respectively. The small velocity separation between the peaks suggests that the two emissions are related. The velocity separation is also consistent with two different H^{13}CN hyperfine transitions, but one of the two peaks has a velocity larger than $-30\ \text{km s}^{-1}$ and does not fall in our H^{13}CN classification criteria. The location of this source on the $(l - v)$ diagram agrees with the CO distribution when considered as an SiO line. Thus the source is listed here among the SiO line detections. In Sgr B2, other double peaked profiles have been seen in SiO emission with line widths of $\sim 100\ \text{km s}^{-1}$ and at velocities from ~ -25 to $\sim 100\ \text{km s}^{-1}$ (Martin-Pintado et al. 1997). The SiO emission in #94 may not be associated with the circumstellar envelope close to the star as in all other cases, as its profile may be more typical to that of bipolar molecular outflows.

#117

See the discussion in Sect. 3.4.

#288

We detected a $14.7\ \text{km s}^{-1}$ wide line at a velocity of $-66.6\ \text{km s}^{-1}$ with respect to SiO (or 269.4 with respect to H^{13}CN), which we classified as likely being an H^{13}CN line. However, Fig. 12 shows that the point if regarded as H^{13}CN is far from any CO emission. The source, $(l, b) = (358.779^\circ, 0.227^\circ)$, is located in the region of the X-ray transient (EXS17379–2952), a region of interest to many other observers. In that region, Durouchoux et al. (1998) detect a few dense CO molecular clouds, of which one at a velocity of $-60\ \text{km s}^{-1}$. We suggest that the SiO line at the position of #288 has an interstellar origin and is associated with the CO cloud of Durouchoux et al. (1998).

#423

At the position of #423 we detected a line which according to our criteria is an H^{13}CN line. This is the only detection outside the Galactic centre region, at a longitude of 23 degrees, that is found at high negative velocity, $-204.7\ \text{km s}^{-1}$ (with respect to SiO) and with a fairly wide line width ($22\ \text{km s}^{-1}$). Its position as SiO line does not fit the velocity-longitude diagram (it does fit when regarded as H^{13}CN emission, then at velocity $131.3\ \text{km s}^{-1}$), and Izumiura et al. (1999) searched for 43 GHz SiO maser without any success. The MSX maps do not show any extended mIR emission or dark region at that position that could suggest the presence of a cloud, however CO maps show a strong concentration of molecular matter (Dame et al. 2001). Also IRAS detected a mIR source, IRAS18302–0848, within $10''$ from the MSX position, and with IRAS flux densities consistent with the MSX flux densities. For this highly reddened source, Stephenson (1992) found a strong excess (4–5 magnitudes) in the $R - I$ colour and absence of molecular bands in the I -spectrum, and concluded that any intrinsic contribution to the redness should be small.

Following his conclusion, that IRAS 18302–0848 is a distant luminous star (which has also been supported by Creese et al. 1995), we conclude that #423 is not an 86 GHz SiO maser emitter and that the origin of reddening of this star is also the origin of the H^{13}CN emission we detected.

5. Conclusions

We have observed 441 colour-selected ISOGAL and MSX sources in the Inner Galaxy ($30^\circ < l < -4^\circ$ and $|b|$ mostly < 1), in the SiO ($v = 1, J = 2 \rightarrow 1$) maser transition and detected 271 lines. We thereby obtained 255 new line-of-sight velocities which doubles the number of maser line-of-sight velocities known in the region we surveyed. To search for 86 GHz ($v = 1$) SiO maser lines in colour-selected mIR sources has proven to be an efficient way to obtain stellar radial velocities in the Inner Galaxy. In the central 2 degrees we notice some confusion with interstellar H^{13}CN emission, but usually the interstellar H^{13}CN and the stellar SiO line can be separated well by using their radial velocities and line widths. The SiO maser emission was

detected towards 61 % of our sources, objects which lie in a transition region of the IR-colour space between Mira and OH/IR stars. The SiO maser detectability decreases with decreasing mIR flux density. We observed 15 sources from the sample of LPV stars by Glass et al. (2001) and found 86 GHz SiO maser emission in 11 of them (73 %), while only 23 % of the LPV stars which follow our selection criteria show OH maser emission. Therefore 86 GHz SiO maser emission is more frequent than OH maser emission. In a later study we will use our new catalogue of stellar line-of-sight velocities for a quantitative analysis of stellar kinematics and SiO maser properties in the Inner Galaxy.

Acknowledgements. We thank D. Levine and M. Morris for sharing their experience about preliminary observations of SiO masers with the IRAM 30m telescope. We are grateful to Ute Lisenfeld, Frank Bertoldi, and the IRAM staff for their support in the observations, most of which were made possible only through the flexible observing mode recently introduced at the 30m telescope. We thank Frederic Schuller for his help with the ISOGAL data. Many thanks to Martin Bureau for fruitful discussions on stellar galactic dynamics. This work was carried out in the context of EARA, the European Association for Research in Astronomy. LOS acknowledges support from the European Commission under contract HPRI-CT-1999-00045. The work of MM is funded by the Netherlands Research School for Astronomy (NOVA) through a *netwerk 2, Ph.D. stipend*.

References

- Alard, C. 2001, *A&A*, 379, L44
 Alard, C., Blommaert, J. A. D. L., Cesarsky, C., et al. 2001, *ApJ*, 552, 289
 Alcolea, J., Bujarrabal, V., & Gallego, J. D. 1989, *A&A*, 211, 187
 Bally, J., Stark, A. A., Wilson, R. W., & Henkel, C. 1988, *ApJ*, 324, 223
 Baud, B., Habing, H. J., Matthews, H. E., & Winnberg, A. 1979, *A&AS*, 35, 179
 Beichman, C. A., Chester, T. J., Skrutskie, M., Low, F. J., & Gillett, F. 1998, *PASP*, 110, 480
 Blommaert, J. A. D. L., van Langevelde, H. J., & Michiels, W. F. P. 1994, *A&A*, 287, 479
 Blum, R. D., Sellgren, K., & Depoy, D. L. 1996, *AJ*, 112, 1988
 Bujarrabal, V. 1994, *A&A*, 285, 953
 Bujarrabal, V., Alcolea, J., Sanchez Contreras, C., & Colomer, F. 1996, *A&A*, 314, 883
 Bujarrabal, V., Planesas, P., & del Romero, A. 1987, *A&A*, 175, 164
 Creese, M., Jones, T. J., & Kobulnicky, H. A. 1995, *AJ*, 110, 268
 Dame, T. M., Hartmann, D., & Thaddeus, P. 2001, *ApJ*, 547, 792
 Dayal, A. & Bieging, J. H. 1995, *ApJ*, 439, 996
 Debattista, V. P., Gerhard, O., & Sevenster, M. N. 2002, *MNRAS* accepted (astro-ph/0203375)
 Deguchi, S., Fujii, T., Izumiura, H., et al. 2000a, *ApJS*, 130, 351
 —. 2000b, *ApJS*, 128, 571
 Deguchi, S., Fujii, T., Miyoshi, M., & Nakashima, J. 2002, *PASJ*, 54, 61
 Durouchoux, P., Vilhu, O., Corbel, S., et al. 1998, *ApJ*, 507, 781
 Egan, M. P., Price, S. D., Moshir, M. M., et al. 1999, *AFRL-VS-TR-1999*, 1522
 Epchtein, N., de Batz, B., Copet, E., et al. 1994, *Ap&SS*, 217, 3
 Felli, M., Comoretto, G., Testi, L., Omont, A., & Schuller, F. 2000, *A&A*, 362, 199
 Fukui, Y., Iguchi, T., Kaifu, N., et al. 1977, *PASJ*, 29, 643
 Fux, R. 1999, *A&A*, 345, 787
 Glass, I. S. 2000, *The Observatory*, 120, 153
 Glass, I. S., Matsumoto, S., Carter, B. S., & Sekiguchi, K. 2001, *MNRAS*, 321, 77
 Habing, H. J. 1996, *A&A Rev.*, 7, 97
 Haikala, L. K., Nyman, L.-A., & Forsstroem, V. 1994, *A&AS*, 103, 107
 Hennebelle, P., Pérault, M., Teyssier, D., & Ganesh, S. 2001, *A&A*, 365, 598
 Hirota, T., Yamamoto, S., Mikami, H., & Ohishi, M. 1998, *ApJ*, 503, 717
 Holtzman, J. A., Watson, A. M., Baum, W. A., et al. 1998, *AJ*, 115, 1946
 Imai, H., Deguchi, S., Fujii, T., et al. 2002, *PASJ*, 54, L19
 Izumiura, H., Deguchi, S., Fujii, T., et al. 1999, *ApJS*, 125, 257
 Jiang, B. W. 2002, *ApJ*, 566, L37
 Kwok, S., Volk, K., & Bidelman, W. P. 1997, *ApJS*, 112, 557
 López-Corredoira, M., Cohen, M., & Hammersley, P. L. 2001a, *A&A*, 367, 106
 López-Corredoira, M., Hammersley, P. L., Garzón, F., et al. 2001b, *A&A*, 373, 139
 Lane, A. P. 1982, *Ph.D. Thesis*
 Levine, D. A. 1995, *Ph.D. Thesis*
 Lewis, B. M. 1990, *AJ*, 99, 710
 Lindqvist, M., Winnberg, A., Habing, H. J., & Matthews, H. E. 1992, *A&AS*, 92, 43
 Lindqvist, M., Winnberg, A., Johansson, L. E. B., & Ukita, N. 1991, *A&A*, 250, 431
 Lis, D. C., Serabyn, E., Zylka, R., & Li, Y. 2001, *ApJ*, 550, 761
 Martin-Pintado, J., Bachiller, R., & Fuente, A. 1992, *A&A*, 254, 315
 Martin-Pintado, J., de Vicente, P., Fuente, A., & Planesas, P. 1997, *ApJ*, 482, L45
 Matsuura, M., Yamamura, I., Murakami, H., et al. 2000, *PASJ*, 52, 895
 Messineo, M., Habing, H., Sjouwerman, L., Omont, A., & Menten, K. 2002a, in preparation
 —. 2002b, in preparation
 Miyazaki, A., Deguchi, S., Tsuboi, M., Kasuga, T., & Takano, S. 2001, *PASJ*, 53, 501
 Nakada, Y., Onaka, T., Yamamura, I., et al. 1991, *Nature*, 353, 140

- Nyman, L.-A., Hall, P. J., & Le Bertre, T. 1993, *A&A*, 280, 551
- Nyman, L.-A., Johansson, L. E. B., & Booth, R. S. 1986, *A&A*, 160, 352
- Olnon, F. M., Habing, H. J., Baud, B., et al. 1984, *ApJ*, 278, 41
- Olofsson, H., Lindqvist, M., Nyman, L.-A., & Winnberg, A. 1998, *A&A*, 329, 1059
- Omont, A., Ganesh, S., Alard, C., et al. 1999, *A&A*, 348, 755
- Omont, A. & the ISOGAL collaboration. 2002, in preparation
- Ortiz, R., Blommaert, J. A. D. L., Copet, E., et al. 2002, *A&A*, 388, 279
- Ortwin. 2002, To appear in: *Matter in the Universe*, eds. Jetzer P., Pretzl K., von Steiger R., *Space Science Reviews*, Kluwer.
- Price, S. D., Egan, M. P., Shipman, R. F., et al. 1997, *American Astronomical Society Meeting*, 191
- Schuller, F. & the ISOGAL collaboration. 2002, in preparation
- Schultheis, M., Ganesh, S., Glass, I. S., et al. 2000, *A&A*, 362, 215
- Schultheis, M., Ganesh, S., Simon, G., et al. 1999, *A&A*, 349, L69
- Sevenster, M. N., Chapman, J. M., Habing, H. J., Killeen, N. E. B., & Lindqvist, M. 1997a, *A&AS*, 122, 79
- . 1997b, *A&AS*, 124, 509
- Sevenster, M. N., van Langevelde, H. J., Moody, R. A., et al. 2001, *A&A*, 366, 481
- Shiki, S., Ohishi, M., & Deguchi, S. 1997, *ApJ*, 478, 206
- Sjouwerman, L. O., Lindqvist, M., van Langevelde, H. J., & Diamond, P. J. 2002a, submitted to *A&A*
- Sjouwerman, L. O., Messineo, M., & Habing, H. 2002b, in preparation
- Sjouwerman, L. O., van Langevelde, H. J., Winnberg, A., & Habing, H. J. 1998, *A&AS*, 128, 35
- Stanek, K. Z., Mateo, M., Udalski, A., et al. 1994, *ApJ*, 429, L73
- Stephenson, C. B. 1992, *AJ*, 103, 263
- Teyssier, D., Hennebelle, P., & Pérault, M. 2002, *A&A*, 382, 624
- Unavane, M. & Gilmore, G. 1998, *MNRAS*, 295, 145
- van der Veen, W. E. C. J. & Habing, H. J. 1988, *A&A*, 194, 125
- Vauterin, P. & Dejonghe, H. 1998, *ApJ*, 500, 233
- Weinberg, M. D. 1992, *ApJ*, 384, 81
- Whitelock, P. 1992, in *ASP Conf. Ser. 30: Variable Stars and Galaxies*, 11
- Zhao, H., Spergel, D. N., & Rich, R. M. 1994, *AJ*, 108, 2154